JOURNAL OF MATERIALS SCIENCE 32 (1997) 5295–5304

Dissolution of quartz in vitrified ceramic materials

M. J. JACKSON
Unicorn Abrasives, Central Research and Development Laboratory, Tuffley Crescent, Gloucester GL1 5NG, UK

B. MILLS
School of Engineering and Technology Management, Liverpool John Moores University, Byrom Street, Liverpool L3 3AF, UK

The dissolution of quartz in vitrified ceramic materials was investigated. A mathematical model was derived and compared with published data and experimental data using X-ray diffraction techniques. When compared with published experimental data, the model correlated better than other dissolution models. However, over longer periods of heat treatment, the model becomes less accurate. The model may be of practical use in describing various types of kinetic data used by manufacturers of vitrified ceramic materials.

1. Introduction

In a heterogeneous reaction, there is a reaction interface between the reacting phases; this may be between a nucleus and the matrix in a solid–solid system, or a crystal and the molten phase in a liquid–solid system. When considering the kinetics of liquid–solid reactions, the rate of dissolution of a solid phase is particularly important when a mixture of solids are converted to liquid phases, or when the corrosion of refractory solids is effected by a liquid phase. For a reaction to proceed, three stages are required: the first is material transport to the interface; the second is reaction at the phase boundary; and the third is material transport of the reacted products away from the reaction interface. Reactions at the interface also absorb or liberate heat, thus changing boundary temperatures and limiting the rate of the process. Any of these processes determines the overall rate of the process, because the overall reaction rate is determined by the slowest of these series of steps.

The dissolution of quartz in a liquid phase does not require a nucleation step. One process that determines the rate of the overall reaction is the phase-boundary reaction rate which is fixed by the movement of ions across the interface. However, reaction at the phase boundary leads to an increased concentration at the interface. Ions must diffuse away from the reaction interface so that the reaction continues. The rate of material transfer and the diffusion rate is controlled by molecular diffusion in the presence of a high-viscosity liquid phase.

For a stationary solid in an unstirred liquid, or in a liquid with no fluid flow produced by hydrodynamic instabilities, the rate of dissolution is governed by molecular diffusion. The effective diffusion length over which mass is transported is proportional to $(Dt)^{1/2}$ [1], and therefore the change in thickness of the solid, which is proportional to the mass dissolved, varies with $t^{1/2}$. In reaction systems which involve convection due to hydrodynamic instabilities from density gradients which arise from thermal gradients, or from concentration gradients due to dissolution, the initial dissolution kinetics should be governed by molecular diffusion.

Natural, or free, convection occurs because of hydrodynamic instabilities in the liquid which gives rise to fluid flow over the solid. This enhances the kinetics of dissolution. It has often been observed in the processing of metals that the amount of dissolution is dependent on whether or not the solid body is totally immersed in the liquid. Generally, a partially submerged solid undergoes more dissolution near the solid–liquid interface which, in metal processing terms, is called the metal line. Below this interface the kinetics of corrosion of the solid can be analysed using the principles of free convection. After a relatively short period of time, during which the kinetics of molecular diffusion prevail, the rate of dissolution becomes less dependent on time. The general equation for mass transport during convection is:

$$j = \frac{\mathrm{d}n/\mathrm{d}t}{A} = \frac{D(c_i - c_\infty)}{\delta(1 - c_i\bar{V})} \quad (1)$$

where j is the number of moles per second per square centimetre removed, c_∞ is the concentration in the bulk liquid, c_i is the saturation concentration at the

interface, δ is the boundary-layer thickness, D is the effective diffusion coefficient through the boundary layer, and $\bar{V}$ is the partial molar volume. The boundary layer is shown in Fig. 1 and is defined by

$$\delta = \frac{c_i - c_\infty}{(\mathrm{d}c/\mathrm{d}y)} \tag{2}$$

where $(\mathrm{d}c/\mathrm{d}y)$ is the concentration gradient at the interface. The boundary-layer thickness is determined by the hydrodynamic conditions of fluid flow. Viscous liquids form much thicker boundary layers which tends to impede material transfer. Higher liquid velocities promote the formation of thinner boundary layers and permit more rapid material transfer. For refractory dissolution in glass materials and silicate slags, the high viscosity and slow fluid flows combine to give thick boundary layers. Boundary-layer thicknesses may be as large as 1 cm, or in rapidly-stirred aqueous solutions as low as a few micrometres. Also, the diffusion rate is much slower in viscous silicate liquids than in aqueous solutions, thus giving a tendency for the reaction process to be controlled by material-transfer phenomena rather than by interface reactions.

The fraction of quartz remaining in vitrified ceramic materials is important when considering the heat treatment of ceramic bodies. Early investigations on the dissolution of quartz focused on using porcelain bodies as the model material [2, 3]. The fraction of quartz remaining as a function of firing time was studied by Krause and Keetman [4], Hamano [5], Mattyasovsky-Zsolnay [6], and Monshi [7]. Considerable data was generated by Lundin [8] using X-ray diffraction techniques to measure residual quartz contents in whiteware bodies. Lundin [8] attempted to fit the relationships derived as functions of time to his data, but without success. Lundin [8] explained the difficulty in developing a realistic model. The difficulty arises from the fact that the phase boundary between quartz and melt moves during the diffusion process. The problem of a fixed boundary can be solved without difficulty, although this is not equivalent to actual conditions.

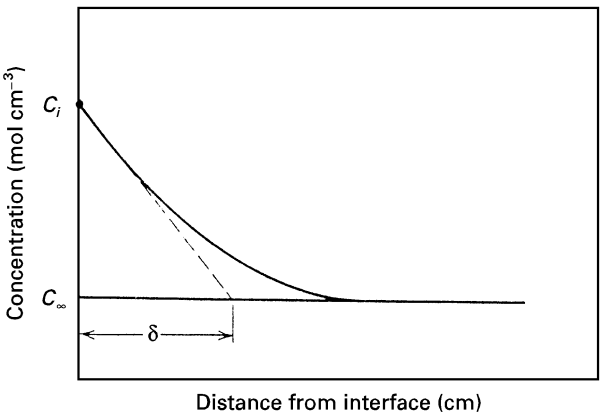

Figure 1 Concentration gradient through the diffusion layer at the solution interface.

2. Dissolution model

The dissolution model assumes that at a constant absolute temperature, T, a particle of quartz melts in the surrounding viscous melt, and that the rate of change of the volume of quartz, $\mathrm{d}v$, is proportional to the volume of the quartz, v, present in the melt, at that instant in time, i.e.

$$\frac{\mathrm{d}v}{\mathrm{d}t} \propto v \tag{3}$$

The above assumption is based on the fact that alkali ions diffuse from the viscous melt to the quartz particle boundary, thus producing a dissolution rim around each quartz particle. A high reaction rate will initially occur which continuously decreases as the quartz particle will be converted to a viscous melt.

Previous work on quartz dissolution in whiteware bodies considered spherical quartz particles with an average diameter. With an increase in time at a constant temperature, the radius of the particles decreases. The equation relating the original radius of the particle and its penetration depth is

$$r' = r - \Delta r \tag{4}$$

where r' is the particle radius at any point in time, r is the original particle radius, and Δr is the penetration depth. Fig. 2 shows a quartz particle with a penetration depth, Δr. The penetration depth is equivalent to the diffusion distance for the movement of alkali ions during time, t, from the start of the reaction. As time proceeds, Δr increases as r' reduces which results in

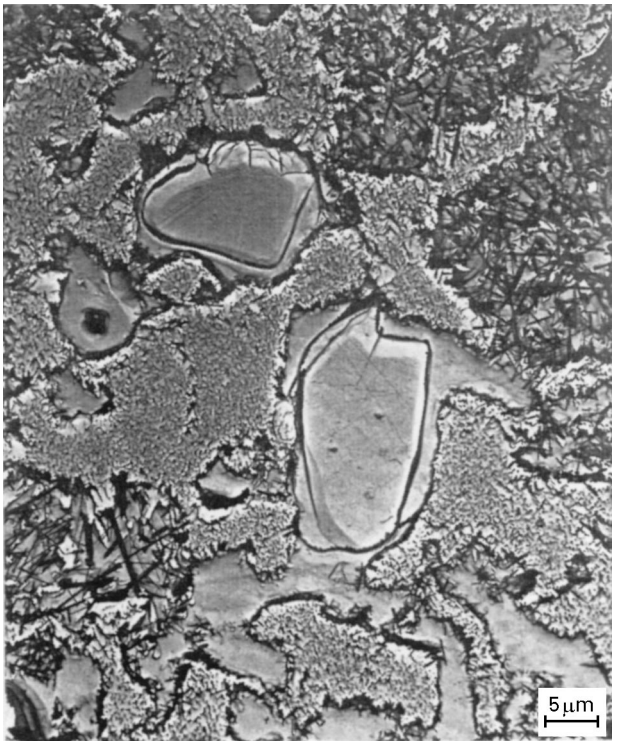

Figure 2 Scanning electron micrograph of a whiteware body of composition 50 wt% clay, 25 wt% quartz, and 25 wt% feldspar. The silica replica was etched for 10 s in 40% hydrofluoric acid etch solution [8]. The figure shows a partially dissolved quartz particle with surrounding dissolution rim.

a decrease in the volume of quartz remaining and a reduction in the dissolution rate.

It is assumed that the reaction rate is inversely proportional to the original particle-size distribution and the penetration depth. This assumes that quartz particles have a relatively complicated particle-size distribution, hence

$$\frac{dv}{dt} \propto \frac{1}{a\Delta r} \tag{5}$$

where a is a constant related to the original particle-size distribution. The constant of proportionality is related to the diffusion coefficient at a temperature, T, owing to the diffusion-controlling mechanisms of alkali-ion mobility from the reaction boundary. Equating Equations 3 and 5 and introducing the diffusion constant, D_T, and a constant, u, to ensure dimensional homogeneity, yields the differential equation

$$\frac{dv}{dt} = -uD_T \frac{V}{a\Delta r} \tag{6}$$

The negative coefficient indicates a decrease in quartz volume as time, dt, increases in magnitude. The temperature dependence of diffusion is expressed by Arrhenius's equation,

$$D_T = D_o.e^{-Q/RT} \tag{7}$$

where D_o is a constant for the given chemical state, Q is the experimental activation energy for diffusion of species, R is the universal gas constant, and T is absolute temperature.

Fick's law states that diffusion distance, Δr, is a function of time and absolute temperature, and is described by the equation

$$\Delta r \approx (D_T\, t)^{1/2} \tag{8}$$

Substituting values of D_T and Δr from Equations 7 and 8 into Equation 6 yields

$$\frac{dv}{v} = -\frac{u}{a} D_o^{1/2} \exp\left(\frac{-Q}{2RT}\right) \frac{dt}{t^{1/2}} \tag{9}$$

The above differential equation can be integrated assuming that, at an isothermal temperature, T, the original volume fraction, V, at zero time changes to a final volume, v, after time duration, t. Hence

$$\int_V^v \frac{dv}{v} = -\frac{u\,D_o^{1/2}}{a} \exp\left(\frac{-Q}{2RT}\right) \int_0^t \frac{dt}{t^{1/2}} \tag{10}$$

The principal equation then becomes

$$\ln\left(\frac{v}{V}\right) = -\frac{u\,D_o^{1/2}}{a} t^{1/2} \exp\left(\frac{-Q}{2RT}\right) \tag{11}$$

Grouping the constants together gives,

$$A = \frac{u\,D_o^{1/2}}{a} \tag{12}$$

$$B = \frac{Q}{2R} \tag{13}$$

The constants shown above can be evaluated using two values of volume of quartz at the same, or at different, soaking times at two different temperatures, T_1 and T_2. The two equations can then be solved simultaneously,

$$\ln\left(\frac{v_1}{V}\right) = -A\, t_1^{1/2} \exp\left(\frac{-B}{T_1}\right) \tag{14}$$

and

$$\ln\left(\frac{v_2}{V}\right) = -A\, t_2^{1/2} \exp\left(\frac{-B}{T_2}\right) \tag{15}$$

From Equations 14 and 15, the constant B is expressed

$$B = \left(\frac{T_1 T_2}{T_1 - T_2}\right) \ln\left[\frac{\ln\left(\frac{v_1}{V}\right)}{t_1^{1/2}} \Big/ \frac{\ln\left(\frac{v_2}{V}\right)}{t_2^{1/2}}\right] \tag{16}$$

The volume of quartz remaining after a period of heat treatment at the soaking temperature is

$$v_{T,t} = V \exp\left[-A\, t^{1/2} \exp\left(\frac{-B}{T}\right)\right] \tag{17}$$

The mass fraction of quartz, m, is the usual measure of quartz remaining after a period of heat treatment when using X-ray methods of determination. Expressing Equation 17 in terms of mass fraction yields

$$\frac{m_{T,t}}{\rho_{\beta\text{-quartz}}} = \frac{M}{\rho_{\alpha\text{-quartz}}} \exp\left[-At^{1/2} \exp\left(\frac{-B}{T}\right)\right] \tag{18}$$

The density, ρ, of α-quartz is 2651 kgm^{-3}, and the density of β-quartz is 2640 kg m^{-3} [9]. Grouping the density constants together gives the principal equation for mass fraction

$$m_{T,t} = M\gamma \exp\left[-At^{1/2} \exp\left(\frac{-B}{T}\right)\right] \tag{19}$$

3. Experimental procedure

3.1. Raw materials and material preparation

The raw materials used in the experimental study were Hymod Prima ball clay, standard porcelain China clay, potash feldspar, and synthetic quartz (supplied as silica flour). The chemical analyses of these raw materials appears in Table I. Rational analyses of the raw materials were performed to reveal the mineralogical composition of the raw materials. The rational

TABLE I Chemical analyses of raw materials used in the present work

	China clay	Ball clay	Potash feldspar	Quartz
Al_2O_3 (wt%)	37	31	18.01	0.65
SiO_2 (wt%)	48	52	66.6	98.4
K_2O (wt%)	1.65	1.8	11.01	0.35
Na_2O (wt%)	0.1	0.2	3.2	0.04
CaO (wt%)	0.07	0.2	0.09	0.00
MgO (wt%)	0.03	0.3	0.09	0.00
TiO_2 (wt%)	0.02	0.9	0.00	0.07
Fe_2O_3 (wt%)	0.68	1.1	0.11	0.03
Loss on ignition (wt%)	12.5	16.5	0.89	0.20

analyses appear in Table II. The characteristic X-ray diffraction spectra for ball clay and China clay are shown in Figs 3 and 4.

The raw materials were mixed in a mortar, pressed in a mould, then fired at various soaking temperatures. A heating rate of 2.9 °C min^{-1} was employed until the soaking temperature was achieved. The samples were cooled to room temperature at a rate of 1.8 °C min^{-1} to avoid thermal stress fracture.

3.2. Measurement of the mass fraction of quartz

The dissolution model was compared with experimental data using the X-ray powder diffraction method. X-ray diffraction of the raw materials was performed on a Philips 1710 X-ray generator with a 40 kV tube voltage and a 30 mA current. Monochromatic CuK_α radiation, $\lambda = 0.154\,060$ nm, was employed. A scanning speed of 2 ° min^{-1} for diffraction angles of 2θ was used between 2θ angles of 10° and 80°, and the X-ray intensity was recorded using a computer. The spectrum was then analysed and compared with known spectra.

TABLE II Mineralogical analyses of raw materials used in the present work

	China clay	Ball clay	Potash feldspar	Quartz
Quartz (wt%)	4.05	12.77	4.93	98.40
Orthoclase (wt%)	0.00	15.23	64.96	0.00
Kaolinite (wt%)	79.70	62.71	2.17	0.00
Mica (wt%)	13.94	0.00	0.00	0.00
Soda feldspar (wt%)	0.8	1.69	27.07	0.00
Miscellaneous oxides/losses (wt%)	1.51	7.60	0.87	1.60

Powder specimens were prepared by crushing in a mortar with a pestle in preparation for quantitative X-ray diffraction. To eliminate the requirement of knowing mass absorption coefficients of ceramic samples for quantitative X-ray diffraction, Alexander and Klug [10] introduced the use of an internal standard. Firstly, the ceramic sample is crushed to form a powder – the sizes of particles should be small enough to make extinction and micro-absorption effects negligible. Secondly, the internal standard to be added should have a mass absorption coefficient at a radiation wavelength such that intensity peaks from the phase(s) being measured are not diminished or amplified.

It should be noted that the powder diffraction mixture should be homogeneous on a scale of size smaller than the amount of material exposed to the X-ray beam, and should be free from preferred orientation. The powder bed which is 'X-rayed' should be deep enough to give maximum diffracted intensity.

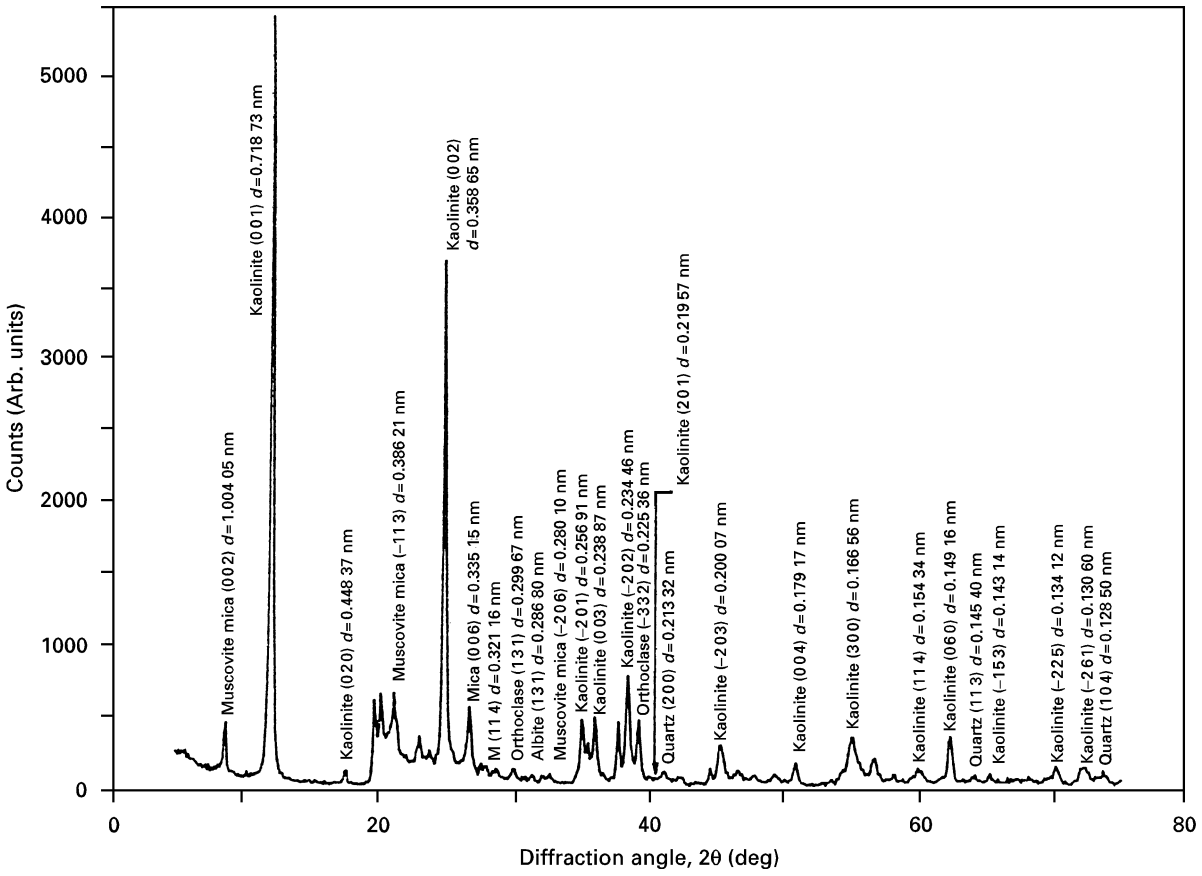

Figure 3 X-ray diffraction spectrum of China clay showing crystallographic planes and interplanar distances of various mineral phases in the clay.

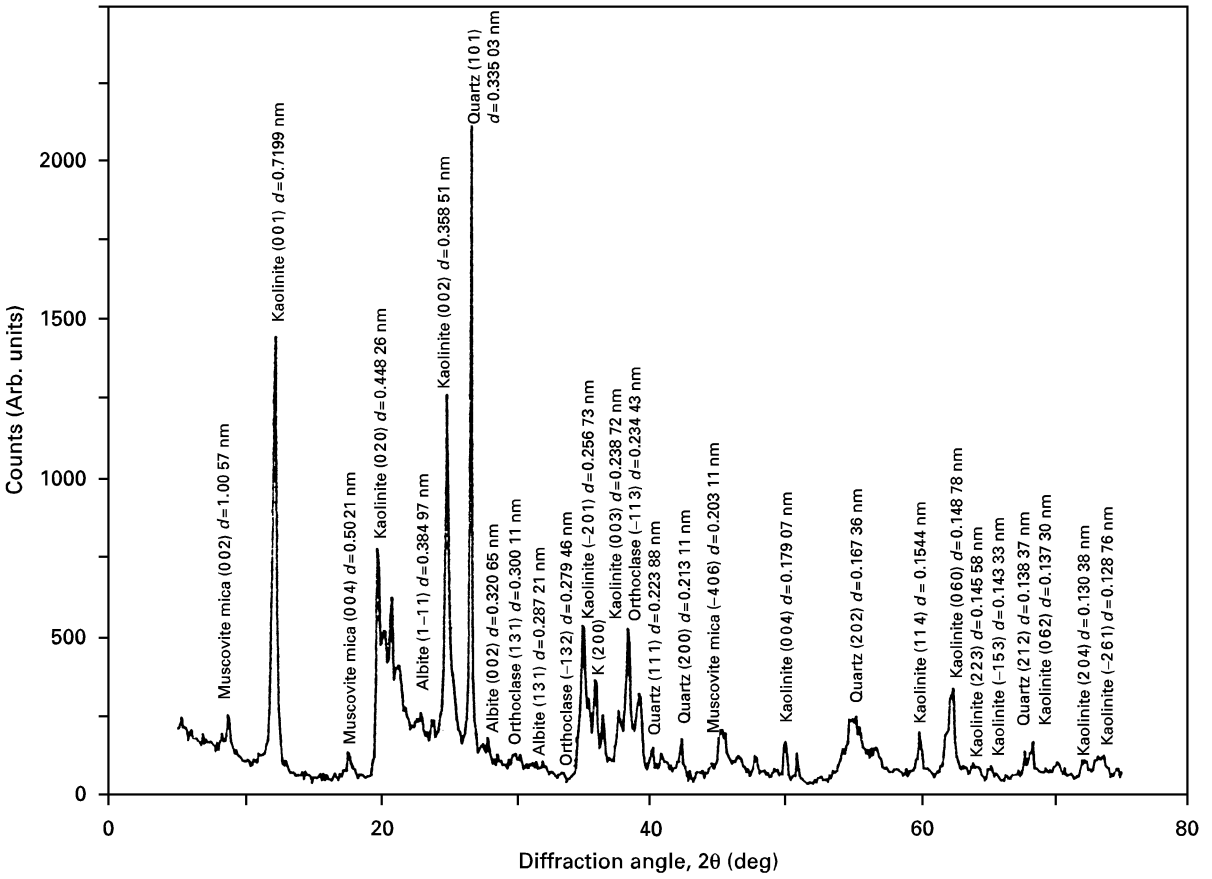

Figure 4 X-ray diffraction spectrum of ball clay showing crystallographic planes and interplanar distances of various mineral phases in the clay.

The expected equilibrium phases from the fired mixtures are quartz (unreacted and partially dissolved), mullite, cristobalite and glass. However, from the samples tested, the compounds quartz, mullite and glass were successfully detected. A calibration curve was constructed using a suitable internal standard (calcium fluoride), a diluent (glass made by melting potash feldspar), and a synthetic form of the phase(s) to be measured. Synthetic mullite had a purity greater than 99.8%, whilst powdered quartz had a purity greater than 99.84% SiO_2. The method used for quantitative analysis was that method espoused by Khandewal and Cook [11].

The internal standard gave a fairly intense (1 1 1) reflection ($d = 0.1354$ nm) lying between the (1 0 0) reflection for quartz ($d = 0.4257$ nm) and the (2 0 0) reflection for mullite ($d = 0.3773$ nm). Using Cuk_α radiation ($\lambda = 0.15405$ nm), the corresponding values of diffraction angle 2θ are: (1 0 0) quartz $= 20.82^\circ$; (1 1 1) calcium fluoride $= 28.3^\circ$; and (2 0 0) mullite $= 32.26^\circ$. Fig. 5 shows the calibration curve generated by varying proportions of calcium fluoride, synthetic quartz and mullite. Mass fractions of the crystalline phases in the mixture can be read from the calibration lines by measuring the intensity ratio of the phase(s) to the internal standard. Fig. 6 shows the diffraction peaks of interest for quantitative analysis lying between 15° and 40° of the diffraction angle 2θ. The figure shows the reflections of the (1 1 1) plane of calcium fluoride, (2 0 0) plane of mullite, and the (1 0 0) plane of quartz. Fig. 7 shows the complete range of planes for the fired mixtures. In order to calculate the

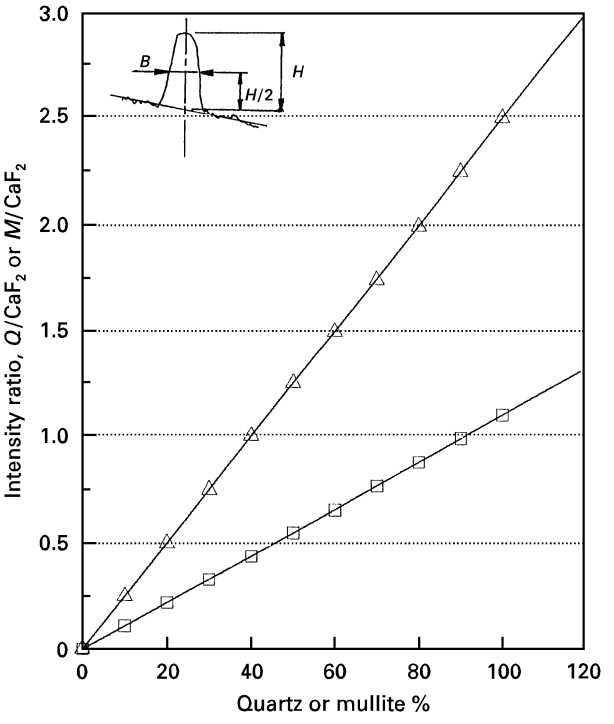

Figure 5 Calibration curve for quantitative analysis of X-ray determined (△) quartz and (□) mullite using the CaF_2 (1 1 1) plane generated by the internal standard.

mass fractions of quartz and mullite in the mixture, the height of the chosen diffraction peak (H) and its width (B) at half-height (H/2) were measured from the diffraction spectrum. The product of these two measures

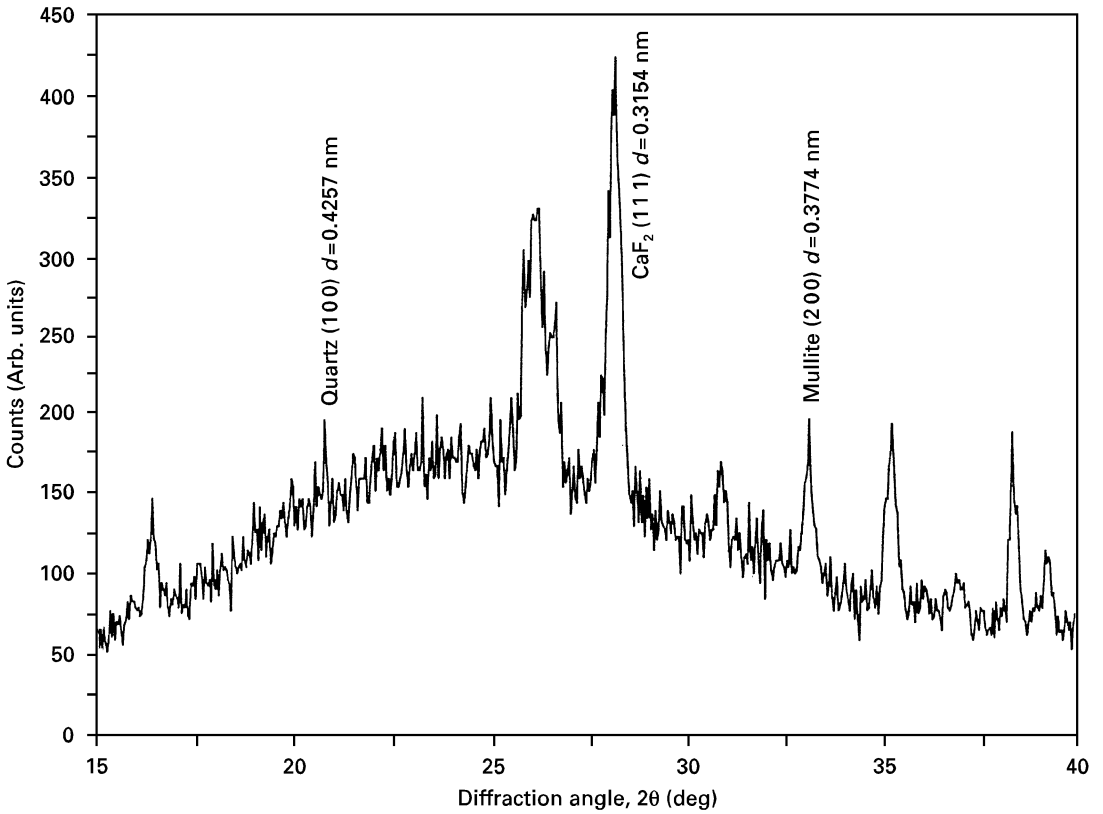

Figure 6 X-ray diffraction spectrum of a heat-treated vitrified ceramic material plus 0.2 g of CaF_2 (internal standard) scanned between the 2θ angles 15° and 40°. The scan rate was 2° min^{-1}. The spectrum shows the characteristic peaks used for quantitative analysis.

was then compared with that of the internal standard, and the resultant intensity ratio was used to find the exact mass fraction of the phase(s) measured in the fired mixtures that were X-rayed.

3.3. Experimental results – verification of the dissolution model

In addition to comparing the experimental results to the dissolution model, results published in the literature were also used to test the accuracy of the model. The composition of the experimental mixtures was matched to those specified by Lundin [8]. Lundin's experimental mixtures were composed of 25 wt% quartz (13.2 μm particle size), 50 wt% clay (kaolin), and 25 wt% flux (potassium feldspar–25 μm particle size).

The initial quartz content of the experimental mixture was 26.36 wt% which, when expressed as an absolute weight and divided by the density of α –quartz, has a volume of 9.943×10^{-3} m^3. Applying Equations 14 and 15 to the experimental data gives

$$\ln\left(\frac{8.863 \times 10^{-3}\text{m}^3}{9.943 \times 10^{-3}\text{m}^3}\right) = -A(2)^{1/2} \exp\left(\frac{-B}{1473K}\right) \quad (20)$$

and

$$\ln\left(\frac{7.803 \times 10^{-3}\text{m}^3}{9.943 \times 10^{-3}\text{m}^3}\right) = -A(2)^{1/2} \exp\left(\frac{-B}{1523\text{K}}\right) \quad (21)$$

where $8.863 \times 10^{-3}m^3$ relates to a quartz content of 23.4 wt%, and $7.803 \times 10^{-3}m^3$ relates to a quartz content of 20.6 wt%. Solving simultaneously yields

$$A = 5.6216 \times 10^8 \quad (22)$$

$$B = 33\,374 \quad (23)$$

from which the experimental activation energy, Q, is 132.65 kcal mol^{-1}. The residual quartz content is

$$m_{T,t} = 26.251 \exp\left[-5.6216 \times 10^8 t^{1/2} \exp\left(\frac{-33\,374}{T}\right)\right] \quad (24)$$

The data comparing Lundin's experimental results, the authors' experimental results, and the dissolution model are shown in Table III. The present model was tested using data published by Lundin and data shown in Table III. When the data are plotted as the logarithm of $[-\ln(m/M)/t^{1/2})$ versus the reciprocal of absolute temperature, $1/T$, then all data points should fit a straight-line relationship. The gradient was calculated to be 33 374, the constant B, using two data points. Lundin's experimental gradient gave a value of 32 962 using the least-squares method, and 34 000 for the present work. The corresponding activation energies for both systems are 131 kcal mol^{-1} for Lundin's work, and 135 kcal mol^{-1} for the present work, respectively. Figs 8 and 9 show the theoretical and

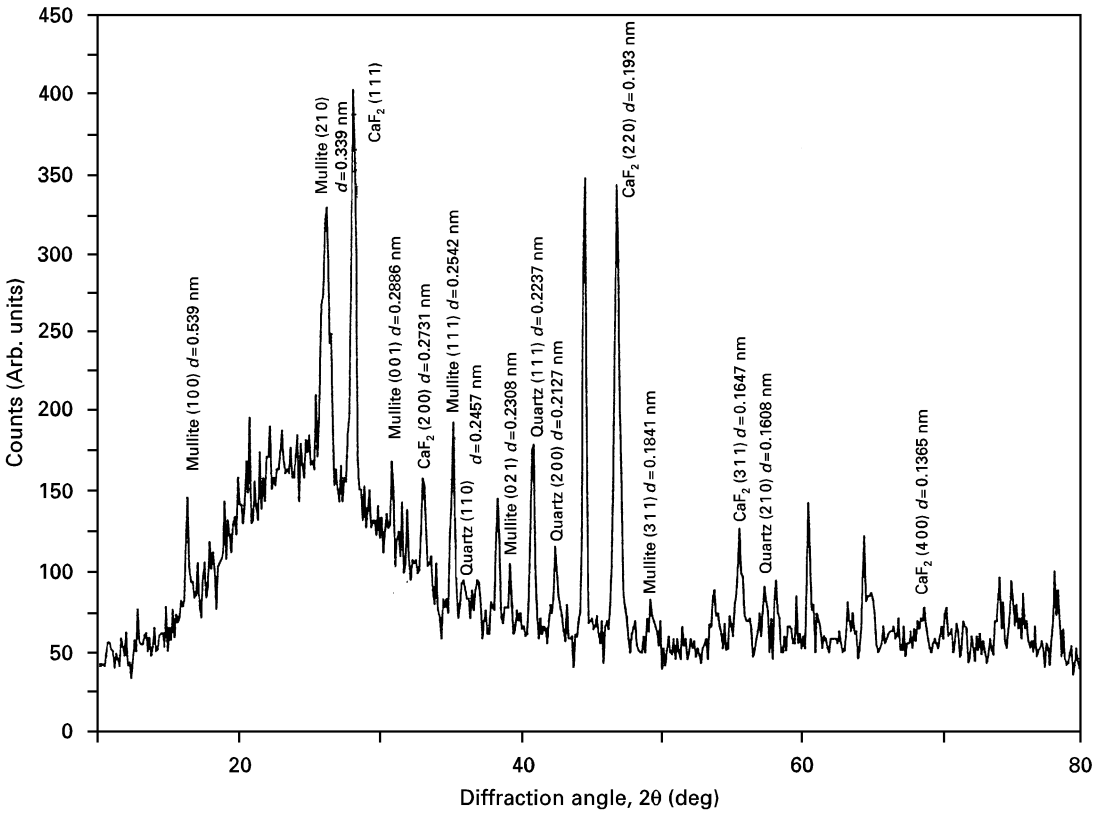

Figure 7 X-ray diffraction spectrum of heat-treated vitrified ceramic material showing interplanar distances of crystallographic planes of mullite, quartz and calcium fluoride. Scan rate was 2° min^{-1}.

TABLE III. Residual quartz content for various heat treatments of Lundin's [8] experimental data compared with the authors' experimental data and the theoretical model

Temperature (°C)	Time (h)	Lundin's experimental result (wt%)	Experimental result (wt%)	Theoretical result (wt%)
1200 (1473 K)	1	24.1	24.2	24.197
1200	1	24.7	24.3	24.197
1200	1	26.1	24.8	24.197
1200	2	23.7	23.8	23.394
1200	2	23.6	23.9	23.394
1200[a]	2	23.4	23.4	23.394
1200	4	21.3	22.2	22.290
1200	8	20.3	20.9	20.854
1200	18	19.0	18.5	18.585
1200	18	18.9	18.6	18.585
1200	48	15.2	15.1	14.94
1250 (1523 K)	1	22.7	22	22.13
1250[a]	2	20.6	20.6	20.613
1250	4	18	18.5	18.645
1250	8	15.5	16	16.175
1250	18	12.6	12.5	12.651
1250	48	8.3	7.8	8.032
1300 (1573 K)	0.5	22.6	20.4	20.59
1300	0.5	21	20.9	20.59
1300	1	20	18.3	18.625
1300	2	16.1	15.9	16.165
1300	4	13.4	12.8	13.253
1300	8	10	9.7	9.94
1300	18	5.9	5.8	6.125
1300	50	1.6	1.8	2.309
1300	120	0.3	0.2	0.603

[a] Values used for deriving the constants used in the theoretical model.

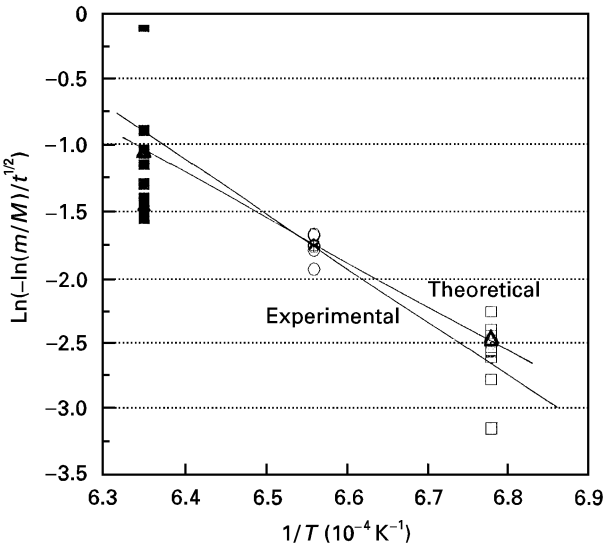

Figure 8 Dissolution behaviour of a clay mixture (25 wt% quartz, 25 wt% feldspar, 50 wt% kaolin) using Lundin's [8] experimental data. (□) Experimental data at 1200 °C; (△) theoretical data at 1200 °C; (○) experimental data at 1250 °C; (∗) theoretical data at 1250 °C; (■) experimental data at 1300 °C; and (▲) theoretical data at 1300°C.

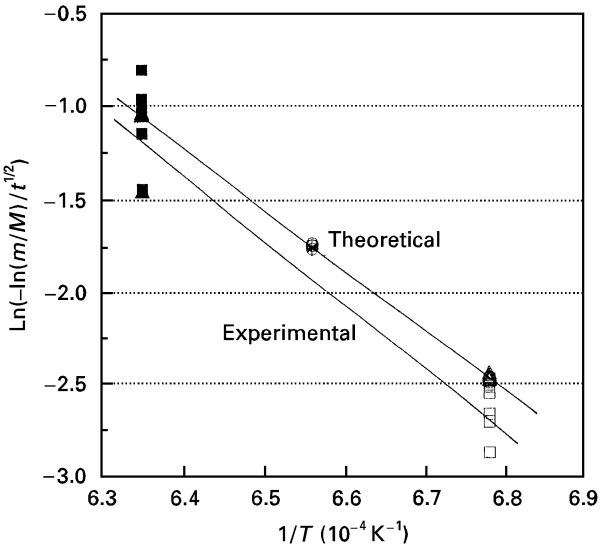

Figure 9 Dissolution behaviour of a clay mixture (25 wt% quartz, 25 wt% feldspar, 50 wt% kaolin) using experimental data from the present work. (□) Experimental data at 1200 °C; (△) theoretical data at 1200 °C; (○) experimental data at 1250 °C; (∗) theoretical data at 1250 °C; (■) experimental data at 1300 °C; and (▲) theoretical data at 1300 °C.

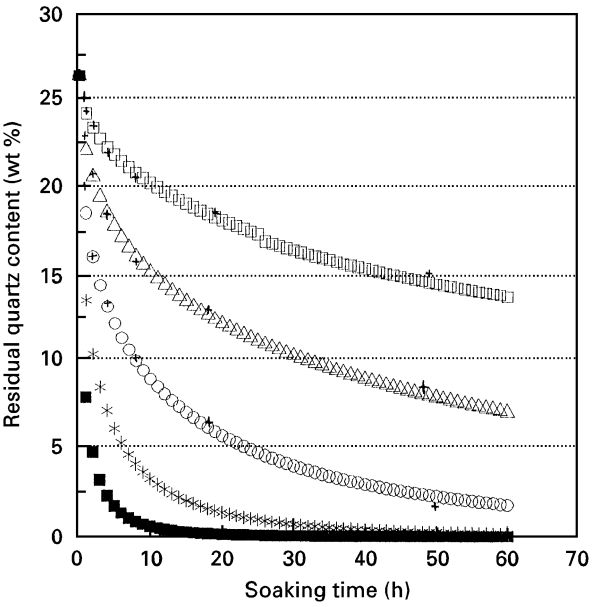

Figure 10 Effect of time on residual quartz content according to the theoretical model and compared with Lundin's experimental data [8]. (□) 1200 °C; (△) 1250 °C; (○) 1300 °C; (∗) 1350 °C; (■) 1400 °C; (+) Lundin's experimental data [8].

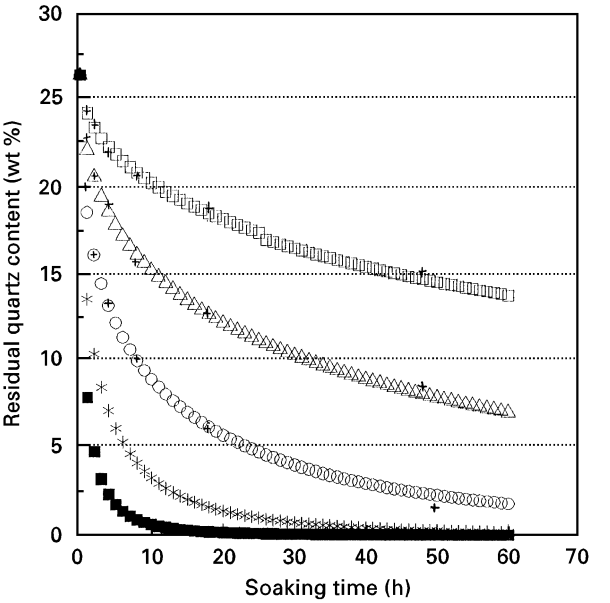

Figure 11 Effect of time on residual quartz content according to the theoretical model and compared with experimental data from the present work. (□) 1200 °C; (△) 1250 °C; (○) 1300 °C; (∗) 1350 °C; (■) 1400 °C; (+) experimental data.

experimental results for Lundin's work and the present investigation. Figs 10 and 11 show the effects of time on residual quartz content at different temperatures according to Equation 24, together with comparative experimental data. Fig. 12 shows the accuracy of the model at various firing temperatures and soaking times.

4. Comparison of dissolution models

A comparison was made with dissolution models published in the literature. One of the earliest models was derived by Jander [12]. The equation can be expressed

$$[1 - (1 - Z)^{1/3}]^2 = \left(\frac{C_1 D}{r^2}\right) t \qquad (25)$$

where Z is the volume of quartz that has been dissolved, r is the original particle radius, and D is the diffusion coefficient for the diffusing species. This equation can be transformed into mass fractions using Archimedes' law, thus

$$\left[1 - \left(\frac{m}{M}\right)^{1/3}\right]^2 = C_2 t \qquad (26)$$

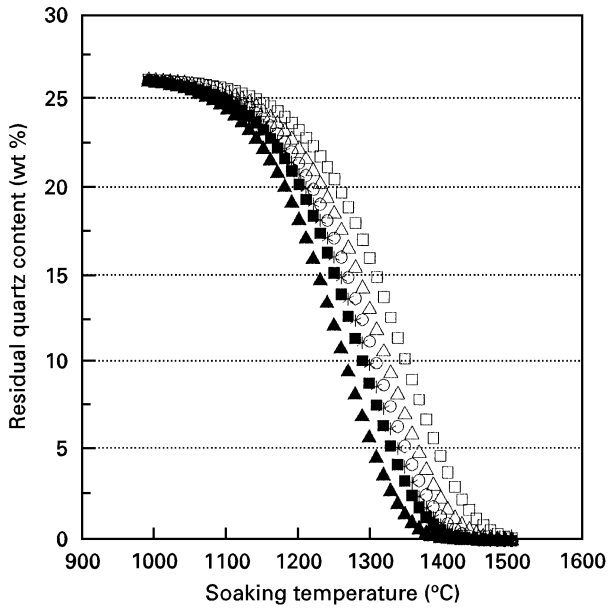

Figure 12 Effect of temperature on residual quartz content according to the theoretical model. (□) 2 h, (△) 4 h, (○) 6 h, (∗) 8 h, (■) 10 h, (▲) 20 h.

where C is a constant dependent on soaking temperature and initial particle size of quartz.

Krause and Keetman [4] expressed the dissolution of quartz as a function of isothermal firing time, i.e.

$$M - m = C_3 \ln t \tag{27}$$

where M is the initial quartz content, m is the residual quartz content after time, t. The unit of time here is seconds such that after 1 s of firing the residual quartz content is equal to the initial quartz content. Mattyasovsky-Zsolnay [6] expressed the dissolution equation in terms of the corrosion of quartz particles, i.e. the thickness of the dissolved layer, as the time-dependent variable

$$r - r' = C_4 \ln t \tag{28}$$

where r is the original particle radius, and r' is the radius of the particle at time t. Transformation of Equation 28 yields

$$1 - \left(\frac{m}{M}\right)^{1/3} = C_5 \ln t \tag{29}$$

Monshi's dissolution model [7] can be transformed into the following equation assuming isothermal firing conditions

$$\ln\left(\frac{m}{M}\right) = -C_6 t^{1/2} \tag{30}$$

The equation of the present model for isothermal firing conditions is transformed into

$$\ln\left(\frac{\gamma m}{M}\right) = -C_7 t^{1/2} \tag{31}$$

where γ is the ratio of densities of β- and α- quartz. Constants for all the equations presented here are calculated using quartz mass fraction data after 18 h firing. The constants are dimensioned in seconds.

The equations shown were compared with experimental data generated by Lundin [8] for a clay-based material containing 40 wt% kaolin, 40 wt% quartz, and 20 wt% feldspar. According to the transformed equations, the mass fraction of quartz can be calculated as follows.

Jander's model [12]

$$m = 41.9[1 - (1.55\,653 \times 10^{-6} t)]^{3/2} \tag{32}$$

Krause and Keetman's model [4]

$$m = 41.9 - (2.5814 \ln t) \tag{33}$$

Mattyasovsky-Zsolnay's model [6]

$$m = 41.9(1 - 0.0287 \ln t)^3 \tag{34}$$

Monshi's model [7]

$$m = \exp(3.735 - 4.5079 \times 10^{-3} t^{1/2}) \tag{35}$$

Present model

$$m = \exp(3.74 - 4.5079 \times 10^{-3} t^{1/2}) \tag{36}$$

The transformed equations are then tested using data provided by Lundin [8]. Referring to Table IV, it can

TABLE IV Residual quartz content for different soaking times at 1300 °C for a fired mixture composed of 40 wt% kaolin, 40 wt% quartz, and 20 wt% feldspar (Lundin's mixture number M21 [8]) compared with other dissolution models

Time (h)	Residual quartz content (wt%)					
	Lundin's experimental data [8]	Jander's model [12]	Krause and Keetman model	Mattyasovsky-Zsolnay's model [6]	Monshi model [7]	Present model
0	41.9	41.9	0.00	0.00	41.9	41.9
0.5	35.9	41.72	22.55	20.26	34.61	34.76
1	32.8	41.54	20.76	18.75	31.97	32.12
2	29.2	41.19	18.97	17.33	28.58	28.72
4	23.2	40.49	17.18	15.98	24.39	24.51
8	19.5	39.11	15.39	14.70	19.49	19.59
18	13.3	35.72	13.30	13.30	13.30	13.36
24	10.7	33.74	12.56	12.81	11.13	11.19
48	6.9	26.18	10.77	11.71	6.43	6.51
120	3.6	7.85	8.96	10.36	2.17	2.17
190	2.7	0.00	7.22	9.72	1.00	1.01
258	2.0	0.00	6.43	9.31	0.54	0.55

be shown that the mass fraction of quartz obtained using the equations derived by Jander [12], Krause and Keetman [4], and Mattyasovsky-Zsolnay [6] did not agree with Lundin's experimental results. The results obtained using Monshi's model [7] are in much better agreement compared to Lundin's data. However, the results obtained from the present model are more accurate at predicting the mass fraction of quartz remaining, owing to the differences in the density of quartz. After long periods of heat treatment, the model predicts lower magnitudes of mass fractions of quartz when compared to Lundin's experimental results.

5. Discussion

A model describing the dissolution of quartz has been derived. However, some of the assumptions made when formulating the model may invalidate the model. It must be borne in mind that in diffusion-controlled processes the total flux at any instant in time is proportional to the total surface area available and the concentration gradient at the interface which is a function of time. The model also assumes that a linear concentration gradient exists across the "spherical shell" of reaction products which does not exist with irregular-shaped quartz particles. The model does obey the parabolic law for diffusion around a sphere which can only apply when the particular sphere has a very low solubility in the solvent. However, this is not the case for silica in most silicate systems. The treatment of the initial size distribution of particles to be dissolved is also inaccurate due to the complexity of size distributions of quartz particles.

The experimental data used to justify the dissolution model do not meet the conditions implicit in the model. The reactions between the three basic components of the model material, i.e. feldspar, kaolinite, and quartz, cannot solely be described as diffusion-controlled dissolution of silica in a liquid phase of constant composition and properties. It therefore seems unlikely that the model can predict the mass fraction of quartz in any silicate system accurately. However, over short soaking times, the results of the model compare well with the experimental results shown in this paper.

6. Conclusions

A dissolution model for the prediction of the mass fraction of quartz in vitrified ceramic materials during heat treatment has been derived. The results predicted by the dissolution model compare well with the experimental results presented in this paper, and fit the data more accurately than other dissolution models. Over longer periods of heat treatment, the model becomes less accurate.

In conclusion, the dissolution model may be of practical use in describing and interpreting various types of kinetic data used by grinding wheel manufacturers and manufacturers of vitrified ceramic products. However, the model cannot be claimed to have a sound theoretical basis.

References

1. P. SHEWMON, "Transformations in Metals" (McGraw-Hill, London, 1969).
2. A. A. KLEIN, *Trans. Am. Ceram. Soc.* **18** (1916) 377.
3. C. W. PARMALEE and C. R. AMBERG, *J. Am. Ceram. Soc.* **12** (1929) 699.
4. P. KRAUSE and E. KEETMAN, Sprechsaal **69** (1936) 45.
5. K. HAMANO, *J. Jpn. Ceram. Soc.* **63** (1955) 432.
6. L. MATTYASOVSKY-ZSOLNAY, *J. Am. Ceram. Soc.* **40** (1957) 299.
7. A. MONSHI, PhD thesis, University of Sheffield, Sheffield (1990).
8. S. T. LUNDIN, "Studies on Triaxial Whitewares" (Almqvist and Wiksell, Stockholm, 1959).
9. O. SAMSONOV, "The Oxide Handbook" (Plenum Press, London, 1973).
10. I. E. ALEXANDER and H. P. KLUG, *Anal. Chem.* **20** (1948) 886.
11. S. K. KHANDEWAL and R. L. COOK, *Am. Ceram. Soc. Bull.* **49** (1970) 522.
12. W. JANDER, *Z. Anorg. U. Allgem. Chem.* **163** (1927) 1.

Received 3 April
and accepted 1 May 1997